In-Situ Study of the Crystallization of Amorphous $CuInSe_2$ Thin Films and the Effect of $InCl_3$ Treatment

Elizabeth Palmiotti[a*], Benjamin Belfore[b], Deewakar Poudel[b], Sylvain Marsillac[b], Angus Rockett[a]

[a] Colorado School of Mines, Golden, CO 80401 U.S.A.

[b] Old Dominion University, Norfolk, VA 23529 U.S.A.

Abstract

Amorphous $CuInSe_2$ films were deposited by rf-magnetron sputtering onto soda-lime glass and silicon substrates. Some were treated with an $InCl_3$ solution. The films were annealed in a nitrogen environment and studied using in-situ high-temperature x-ray diffraction. $CuInSe_2$ recrystallization began at ~270°C and all samples showed increasing crystallinity up to ~380°C. The onset and completion temperatures for crystallization varied minimally between samples. The as-deposited films (no $InCl_3$) showed CuSe phase formation at intermediate temperatures (180-250°C). Na_2O from the soda-lime glass increased the net rate of crystallization. $InCl_3$ resulted in an even greater increase to crystallization rate and largely improved the final crystalline quality.

Keywords: crystallization, kinetics, High-Temperature X-Ray Diffraction, Copper Indium Diselenide, in-situ characterization

1. Introduction

Thin-film photovoltaics offer promise as a low-cost, high-efficiency technology. However, some have a limited commercial presence due to higher manufacturing costs, especially due to expensive, low-throughput capital equipment. Cadmium telluride (CdTe) has the largest market presence of any thin-film due to a high-rate deposition process followed by a rapid

$CdCl_2$ activation treatment, resulting in improved grain size, crystallization, defect passivation, and enhanced device performance [1-4]. Combined, this results in a very fast process that keeps down the capital equipment cost per module, and has allowed CdTe modules to drive the overall cost of photovoltaics down dramatically. Though efficient [5], $CuIn_{(1-x)}Ga_xSe_2$ (CIGS) devices are commercially limited due to typically slow, high-temperature deposition processes. In our previous work we showed that CIGS films co-evaporated at 350°C and 400°C were recrystallized using metal chloride and bromide post-deposition vapor treatments [6,7]. Although the treatments resulted in large grains and improved crystallinity, notable variations to composition and, in most conditions, elimination of the Ga gradient through the film or almost complete loss of Ga resulted. In the results reported here, $CuInSe_2$ (CIS) films were studied to simplify interpretation by avoiding Ga removal by the halide. We present a study of the kinetics of as-deposited and $InCl_3$-enhanced crystallization of amorphous $CuInSe_2$ (CIS) films using high-temperature x-ray diffraction (HT-XRD).

2. Experimental Details

1 μm thick amorphous CIS films were deposited at room temperature by radio-frequency (rf)-magnetron sputtering from a single, 76 mm diameter 99.9% purity CIS target onto soda-lime glass (SLG) and silicon substrates 16.5 cm away. The system was brought to a base pressure of 3.2 mPa and sputtering was conducted in ultra-high purity Ar at 0.25 Pa and 70 W rf power. The as-deposited film composition was 26.9 at% Cu, 22.0 at% In, and 51.1 at% Se.

An Anton Paar DHS-1100 heater stage was installed onto a Malvern Panalytical Empyrean x-ray diffractometer with a Mo x-ray source ($\lambda_{K\alpha}$=0.0711 nm). A polyether ether ketone (PEEK) dome continuously purged with flowing high-purity nitrogen contained the sample on the heater stage. For each heating profile, the temperature was initially increased to 150°C,

stabilized, then a scan was collected. The stage temperature was increased by 10°C at a rate of 60°C per minute, held for one minute, and another scan collected. This was repeated until the stage temperature reached 450°C. Each scan typically took 4.5 minutes.

$InCl_3$ solution treated samples were also studied. A 0.1M $InCl_3$ solution was prepared in methanol. Similar to what is done for the solution $CdCl_2$ treatment of CdTe [8], two drops were placed on the film surfaces, covering the entire surface, and then annealed in an ultra-high purity Ar-purged tube furnace at 55°C for ten minutes to evaporate the methanol. Samples were removed from the tube furnace into laboratory air, immediately transported in a press-fit sample holder, and mounted on the HT-XRD stage. The PEEK dome was immediately installed over the sample and purged with high purity N_2. For surface morphology characterization, after the $InCl_3$ solution was placed on the film surface, the sample was annealed at 55°C for ten minutes then the furnace temperature increased to the desired annealing temperature and held for 10 minutes.

XRD patterns were analyzed and peak parameters extracted using the HighScore Plus software and phases were identified using the International Center for Diffraction Data (ICDD) database [9]. Scanning electron microscopy (SEM) and energy dispersive spectroscopy (EDS) were conducted using a FEI Helios Nanolab 600i FIB-SEM at an accelerating voltage of 10 kV.

3. Results and Discussion

3.1 Ex-Situ Annealing Investigation

Figure 1 shows top-view SEM micrographs of (a) CIS/Si and (b) CIS/SLG annealed at 250°C for 5 minutes each, and (c) CIS/Si and (d) CIS/SLG annealed at 400°C for 5 minutes each in an Ar-purged tube furnace. The samples annealed at 250°C show large hexagonal platelets, identified as CuSe by EDS, on the surface. CuSe platelets have been previously seen in this

temperature range during the annealing of electrodeposited [10] and sputtered [11] CIS films. The samples annealed at 400°C show small particles on the surface that have identical compositions to the CIS film. The compositions of the film before and after annealing were analyzed by EDS and are compiled in Table I.

TOF-SIMS analysis was conducted and revealed Na diffusion from the substrate into the films after annealing. Na is commonly observed in our SIMS measurements of CIS on soda-lime glass at levels that typically scale with grain boundary volume. It is important to note that Na in soda-lime glass is present as Na_2O and some oxygen is typically found in the films as a result, although the two concentrations do not strongly correlate indicating that oxygen mostly escapes from the sample surface.

To demonstrate the morphological evolution resulting from the $InCl_3$ solution treatments, an $InCl_3$ solution treatment was conducted on CIS/Si and CIS/SLG samples then annealed at 350, 400, and 450°C for 10 minutes each in an Ar-purged tube furnace. The resulting SEM micrographs are shown in Figure 2 and composition results in Table I. Large (>0.5 micron) grains formed after $InCl_3$ treatments at all three temperatures. With increasing annealing temperature, the grains are less closely packed. These results differ greatly from the films annealed without $InCl_3$, as shown in Figure 1, which do not show observable grains at similar temperatures even though the films in Figure 2 began as identical amorphous, featureless films. The $InCl_3$ apparently acts as a transport agent to promote accelerated crystallization and grain growth of the material. Cl and O were detected by EDS in all films after treatment as noted in Table I and are discussed in the following section.

The composition of the film changed with increasing temperature, with and without $InCl_3$ solution treatment. Loss of Se was due to the high vapor pressure of Se in the given

experimental conditions. An in-situ treatment procedure has been developed to better control and rectify composition after the introduction of $InCl_3$ [12].

3.2 In-Situ Kinetic Investigation

Figure 3 shows the HT-XRD patterns collected for (a) CIS/Si, (b) CIS/SLG, (c) $InCl_3$ treated CIS/Si, and (d) $InCl_3$ treated CIS/SLG from 150 to 450°C. All samples are amorphous at 150°C, as shown by the broad peak between 10 and 15° for the films on Si, corresponding to the average nearest neighbor spacing of CIS. The films on glass also show a broad peak between 9 and 19° due to the glass substrate, which obscures the amorphous CIS peak. With increasing temperature, the peaks corresponding to the (112), (220/204), and (312/116) plane spacings of $CuInSe_2$ (ICDD Ref. 01-081-1936) at 2θ values 12.19, 19.97, and 23.46°, respectively, appear, sharpen, and increase in intensity. The characteristic peak intensities settle at a near constant value above 380°C for all samples.

As seen in Figures 3(a) and 3(b) for the as-deposited films (no $InCl_3$ treatment), an intermediate CuSe (ICDD Ref. 00-049-1456) phase causes a peak at a 2θ value of 14.2°. The CuSe phase separated and formed the platelets on the film surfaces in Figures 1(a) and 1(b). This phase begins to form at approximately 180°C for both CIS/SLG and CIS/Si, and rapidly grows to a maximum intensity at 240°C. CuSe crystallizes nearly twice as quickly for CIS/SLG compared to CIS/Si based on a comparison of the rate of peak intensity increase over the temperature range of crystallization. Above 240°C the phase is unstable and fully redissolves into the film by 300°C for both samples and only the CIS phase remains. Ouyang et al. showed that a similar phase formation then decomposition occurs for sputtered CIGS films [11]. For CIS/SLG and CIS/Si the increase and sharpening of the characteristic CIS peaks shows that the material is crystallizing and forming small grains not visible by SEM (Figure 1).

The $InCl_3$ solution-treated samples showed similar amorphous CIS peaks until crystallization began at approximately 270°C. Above this temperature the CIS peak intensities rapidly increased due to crystallization until 380°C, then stopped increasing. Note that no intermediate CuSe phase formed with the $InCl_3$ treatment. Probably due to the hygroscopic nature of $InCl_3$ some indium oxide and indium oxy-chloride peaks also appeared. This accounts for the relative increase of In and presence of O and Cl in the EDS results (Table I). These oxide phases were not observed for the samples without $InCl_3$ treatment. Although all annealing procedures were conducted in inert environments, the samples were exposed to air during loading into the HT-XRD system and the $InCl_3$ on the surface likely absorbed oxygen. However, the CIS crystallization trends for these samples behaved as expected and the oxide was concluded not to have impacted the crystallization kinetic data, described below.

Raw peak height values, in counts, and a five-point moving average of full-width at half maximum (FWHM) values for the (112) orientation were plotted versus temperature for CIS/Si (black squares), CIS/SLG (blue triangles), $InCl_3$ treated CIS/Si (red circles), and $InCl_3$ treated CIS/SLG (green downward triangles) (Figures 4(a) and 4(b), respectively). Although data was collected starting at 150°C, data was plotted and analyzed starting at 230°C, which was the first temperature where a reliable (112) peak could be distinguished due to the amorphous nature of the low-temperature range. Diffraction of the amorphous phase is not relevant to the crystallization analysis.

All curves show a minimal change in the CIS peaks up to approximately 270°C. From approximately 270°C to 380°C peak height increases rapidly for all samples and represents when crystallization is occurring. Above 380°C, no further increase in intensity was observed, suggesting that crystallization was complete, although grains may have continued to evolve without further changes in crystallinity observable by XRD (cf. Figure 2). Peak height and FWHM indicate the regularity of composition and structure in the film, including

any crystalline defects. A sharp, high-intensity peak indicates a highly uniform and well organized crystal free of most defects while a broad, low-intensity peak indicates poor order. Peak height and sharpening were increased for the samples deposited onto SLG and even greater for both $InCl_3$ treated samples suggesting the treatment results in higher crystalline quality. It appears that these samples reach the better crystalline state at a higher rate as well, which shows that both act to accelerate the crystallization process.

The improved crystallinity for samples deposited on SLG is possibly due to the influence of Na_2O diffusing from the SLG during annealing, which is known to influence the crystallinity of CIS [13,14]. At temperatures as low as 157°C, Na is known to diffuse through CIGS by Type C grain boundary diffusion and then by Type C grain boundary and bulk diffusion approaching 323°C [15]. This explains that with greater annealing temperatures, more Na diffuses from the SLG substrate into the CIS. Improved crystallinity and grain growth appear to be enhanced in the presence of $InCl_3$. As noted above, the ultimate grain size was much larger when $InCl_3$ was present (Figure 2), see further discussion below.

All samples begin to show crystallinity at approximately the same temperature, 270°C, and all completed their crystallization by 380°C. This indicates that the crystallization onset is not due to the Na_2O or $InCl_3$ but may be influenced by some other process. As the temperature at which crystallization was complete marks a point where atomic diffusion in CIS is sufficient to complete the formation of the crystalline structure to the extent detectable by XRD. The greater overall XRD peak intensities with Na_2O and $InCl_3$ indicate that the crystals were better organized by 380°C in the presence of those species.

A five-point moving average of the (112) peak height data was normalized from zero to one and plotted in Figure 5 per sample. Sigmoidal curve fits of this data were conducted and are

overlayed in Figure 5 (solid lines). The first derivative was taken of the sigmoidal fits to determine the crystallization rate. This is shown in Figure 6.

The fitted crystallization rate curves shown in Figure 6 can be used to determine a relative activation energy based on the temperature of each peak maximum [16]. These maximum temperature values are compiled in Table II. Some differences in the curve positions are noted. Both samples treated with $InCl_3$ shifted towards lower temperatures which corresponds to a lower activation energy of crystallization. However, such differences may not be significant. Based on the quality of the curve fits and the fluctuations in the data we estimate that the peak temperatures have an error of approximately ±5°C. Therefore, nearly all values obtained are within the estimated error of each other.

The absence of a significant difference in activation energy for crystallization suggests that the rate-limiting step of the reaction is unchanged, which is consistent with the similar onset and termination temperatures for crystallization of each sample. However, the absolute intensity of the peaks above ~400°C increase and the FWHM decrease for both samples deposited on SLG and more so for the samples treated with $InCl_3$, indicating better crystallinity. Furthermore, the rate of crystallization as determined from the slope of the curves in Figure 5 increased for the samples treated with $InCl_3$. We conclude that the $InCl_3$ had a significant impact on the rate of crystallization and the final crystalline quality, although the rate limiting step in the process appears to be unchanged in the activation energy of the key step. Therefore, other factors must have increased the process rate exclusive of the activation energy.

Although the Na_2O and $InCl_3$ both enhance material transport during the crystallization, the $InCl_3$ further accelerates atomic transport resulting in the larger grain sizes (Figure 2). We anticipate that this is due to the Cl^- ions dissociating from the $InCl_3$ and then by etching and

re-depositing atoms, resulting in larger grains growing at a faster rate and better crystalline quality.

4. Conclusions

Substrate and $InCl_3$ effects on amorphous $CuInSe_2$ crystallization were studied using in-situ HT-XRD and ex-situ characterization techniques. Crystallinity improved with temperature for all films between ~270°C and 380°C, with and without $InCl_3$, on silicon and glass substrates. This reveals that crystallization temperature is independent of the Na_2O and $InCl_3$. In the absence of $InCl_3$, very little grain growth was observed, although XRD showed that CIS crystals had formed. The reaction rate was accelerated in the presence of $InCl_3$ and large grains were observed for films annealed at 350°C or higher. We note that for post-deposition treatments, NaF is a preferred Na source but does not appear to produce the scale of grain growth observed here [17]. NaCl has also been considered but shows no effect on grain size. Likewise, films with excess In do not exhibit large grain growth. Rather, In deficiency promotes grain growth [18]. Therefore, it appears that neither In nor the Cl alone are key factors in increasing grain size. It is the combination that is critical. $InCl_3$ also inhibits formation of CuSe on the film surface, presumably due to reaction of In with the CuSe to contribute to formation of CIS.

Acknowledgements

This material is based upon work supported by the U.S. Department of Energy's Office of Energy Efficiency and Renewable Energy (EERE) under Solar Energy Technologies Office (SETO) Award Number DE-EE0007551.

References

[1] B. E. McCandless, I. Youm, and R.W. Birkmire, Optimization of vapor post-deposition processing for evaporated CdS/CdTe solar cells, Progress in Photovoltaics: Research and

Applications 7 (1999) 21-30, DOI: 10.1002/(SICI)1099-159X(199901/02)7:1<21::AID-PIP244>3.0.CO2-D.

[2] T. X. Zhou, N. Reiter, R. C. Powell, R. Sasala, and P. V. Meyers, Vapor chloride treatment of polycrystalline CdTe/CdS films, Conference Record of the IEEE Photovoltaic Specialists Conference 1 (1994) 103-106, DOI: 10.1109/WCPEC.1994.519818.

[3] B. E. McCandless, H. Hichri, G. Hanket, and R. W. Birkmire, Vapor phase treatment of CdTe/CdS thin films with $CdCl_2$:O_2, Conference Record of the Twenty-Fifth IEEE Photovoltaic Specialists Conference (1996) 781-784, DOI: 10.1109/PVSC.1996.564244.

[4] C. S. Ferekides, U. Balasubramanian, R. Mamazza, V. Viswanathan, H. Zhao, and D. L. Morel, CdTe thin film solar cells: Device and technology issues, Solar Energy 77 (2004) 823-830, DOI: 10.1016/j.solener.2004.05.023.

[5] M. Nakamura, K. Yamaguchi, Y. Kimoto, Y. Yasaki, T. Kato, and H. Sugimoto, Cd-free Cu(In,Ga)$(Se,S)_2$ thin-film solar cell with a new world record efficiency of 23.35%, IEEE Journal of Photovoltaics 9 (2019) 1863-1867, DOI: 10.1109/JPHOTOV.2019.2937218.

[6] E. Palmiotti, S. Soltanmohammad, A. Rockett, G. Rajan, S. Karki, B. Belfore, and S. Marsillac, Post-Deposition Recrystallization of Chloride Treated Cu(In,Ga) Se_2 Thin-Film Solar Cells, 2018 IEEE 7th World Conference on Photovoltaic Energy Conversion (WCPEC) (A Joint Conference of 45th IEEE PVSC, 28th PVSEC & 34th EU PVSEC) (2018) 163-166, DOI: 10.1109/PVSC.2018.8547595.

[7] E. Palmiotti, S. Karki, B. Belfore, S. Soltanmohammad, G. Rajan, S. Marsillac, and A. Rockett. Post-Deposition Recrystallization of Co-Evaporated Cu(In,Ga)Se_2 Films by Bromide Vapor Treatments, 2019 IEEE 46th Photovoltaic Specialists Conference (PVSC) (2019) 1863-1866, DOI: 10.1109/PVSC40753.2019.8980803.

[8] H.R. Moutinho, R.G. Dhere, M.J. Romero, C.S. Jiang, B. To, and M.M. Al-Jassim, Recrystallization of PVD CdTe Thin Films Induced by $CdCl_2$ Treatment – A Comparison Between Vapor and Solution Processes, 2008 IEEE 33rd Photovoltaic Specialists Conference (2008), GOVDOC: E 9.17:NREL/CP-520-42512.

[9] S. Gates-Rector and T. Blanton. The Powder Diffraction File: A Quality Materials Characterization Database. Powder Diffr., (2019).

[10] A. Gobeaut, L. Laffont, J.-M. Tarascon, L. Parissi, and O. Kerrec, Influence of secondary phases during annealing on re-crystallization of $CuInSe_2$ electrodeposited films, Thin Solid Films 517 (2009) 4436-4442, DOI: 10.1016/j.tsf.2009.01.043.

[11] L. Ouyang, M. Zhao, D. Zhuang, J. Han, Z. Gao, L. Guo, X. Li, R. Sun, and M. Cao, Annealing treatment of Cu(In,Ga)Se_2 absorbers prepared by sputtering a quaternary target for 13.5% conversion efficiency device, Solar Energy 118 (2015) 375-383, DOI: 10.1016/j.solener.2015.05.019.

[12] B. Belfore, D. Poudel, S. Karki, S. Soltanmohammad, E. Palmiotti, T. Lepetit, A. Rockett, and S. Marsillac. Recrystallization of Cu(In,Ga)Se_2 Semiconductor Thin Films via $InCl_3$ Treatment, Thin Solid Films 735 (2021).

[13] S. Ishizuka, A. Yamada, M. Islam, H. Shibata, P. Fons, T. Sakurai, K. Akimoto, and S. Niki, Na-induced variations in the structural, optical, and electrical properties of $Cu(In,Ga)Se_2$ thin films, Journal of Applied Physics 106 (2009), DOI: 10.1063/1.3190528.

[14] A. Rockett, K. Granath, S. Asher, M.M. Al-Jassim, F. Hanson, R. Matson, B. Basol, V. Kapur, J.S. Britt, T. Gillespie, and C. Marshall, Na incorporation in Mo and $CuInSe_2$ from production processes, Solar Energy Materials and Solar Cells 59 (1999) 255-264, DOI: 10.1016/S0927-0248(99)00026-4.

[15] A. Laemmle, R. Wuerz, T. Schwarz, O. Cojocaru-Mirédin, P. Choi, and M. Powalla, Investigation of the diffusion behavior of sodium in $Cu(In,Ga)Se_2$ layers, Journal of Applied Physics 115 (2014), DOI: 10.1063/1.4871457.

[16] P. Redhead, Thermal Desorption of Gases, Vacuum 12 (1962), DOI: 10.1016/0042-207X(62)90978-8.

[17] G. Rajan, B. Belfore, S. Karki, D. Poudel, H. Kahoui, N. Lanham, E. Palmiotti, S. Soltanmohammad, A. Rockett, and S. Marsillac, Impact of Post-Deposition Recrystallization by Alkali Fluorides on Cu(In,Ga)Se2 Thin-Film Materials and Solar Cells, Thin Solid Films 690 (2019), DOI: 10.1016/j.tsf.2019.137526.

[18] L.-C. Yang, C.Y. Cheng, and J.S. Fang, Characterization of polycrystalline $CuInSe_2$ thin films deposited by sputtering and evaporation as a function of composition, Journal of Physics and Chemistry of Solids 69 (2008), DOI: 10.1016/j.jpcs.2007.07.027.

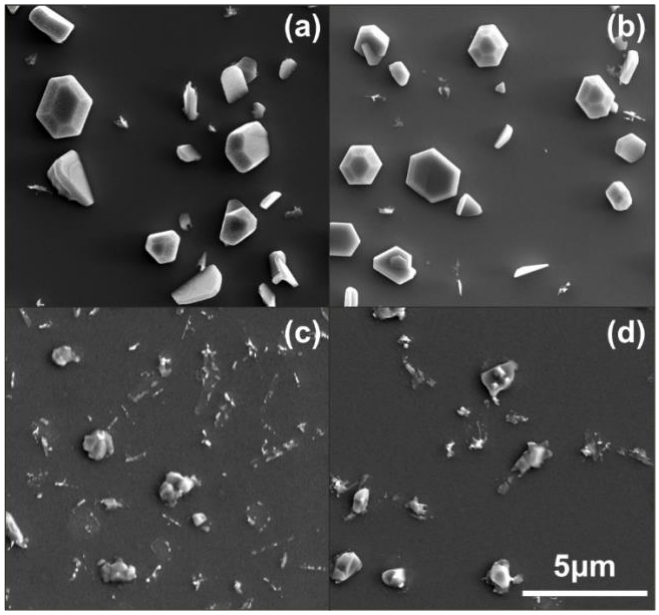

Figure 1: Top-view SEM micrographs of (a) CIS/Si and (b) CIS/SLG after a five minute anneal at 250°C and of (c) CIS/Si and (d) CIS/SLG after a five minute anneal at 400°C.

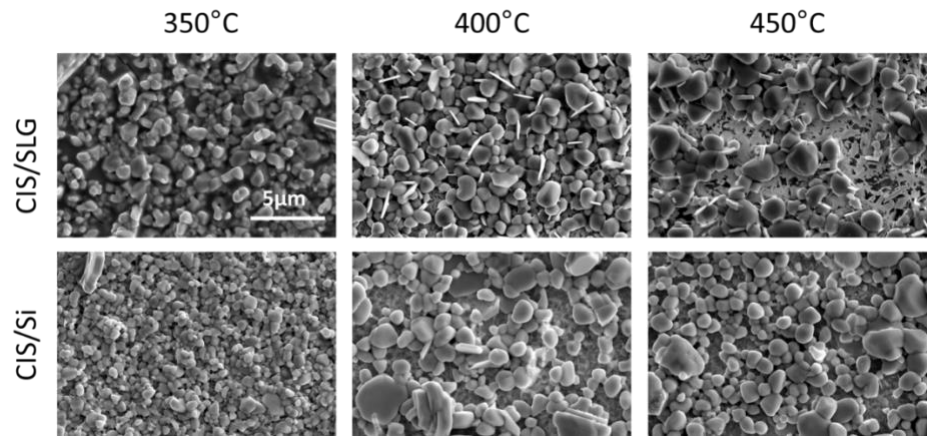

Figure 2: Top-view SEM micrographs of CIS/Si and CIS/SLG films after the $InCl_3$ solution treatments conducted at 350, 400, and 450°C.

At (%)	RT		250°C		400°C	
	As-Deposited		CIS/SLG	CIS/Si	CIS/SLG	CIS/Si
Cu	26.9		21.3	22.2	28.9	32.2
In	22.0		27.0	26.8	27.5	25.6
Se	51.1		50.0	49.4	40.5	39.2
O			1.8	1.6	3.1	3.0
$InCl_3$ Solution Treatments						
	350°C		400°C		450°C	
	CIS/SLG	CIS/Si	CIS/SLG	CIS/Si	CIS/SLG	CIS/Si
Cu	27.1	26.3	27.7	26.2	22.4	28.6
In	18.7	18.4	22.6	25.3	20.8	21.5
Se	37.6	21.9	36.9	37.6	36.3	31.2
O	16.2	21.7	10.8	6.7	19.7	15.6
Cl	0.2	11.7	2.1	4.2	0.8	3.0

Table I: Compositions (at%) of CIS samples after all treatment conditions with and without $InCl_3$.

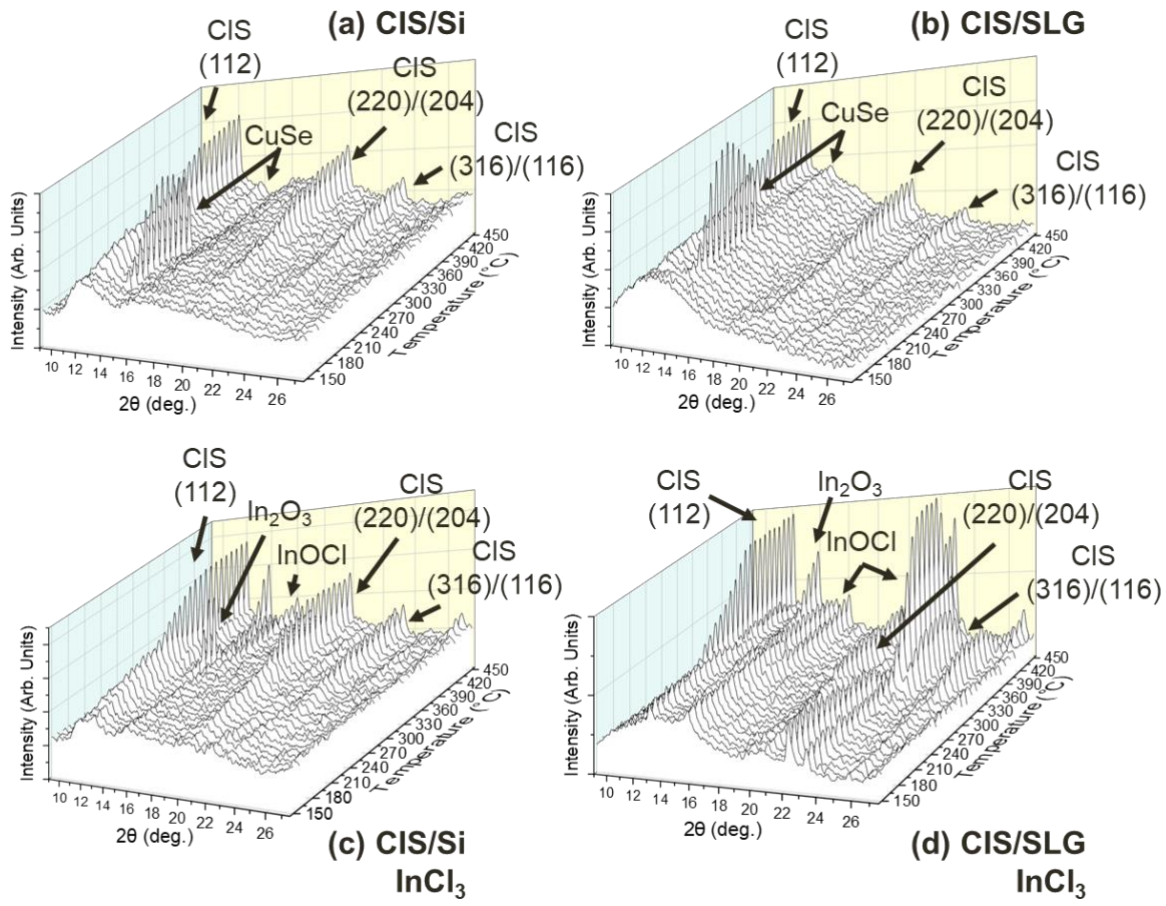

Figure 3: In-situ HT-XRD patterns collected from 150 to 450°C of 1µm thick CIS films on SLG and Si substrates with and without $InCl_3$ solution treatments. Unidentified peaks are parts of the identified phases.

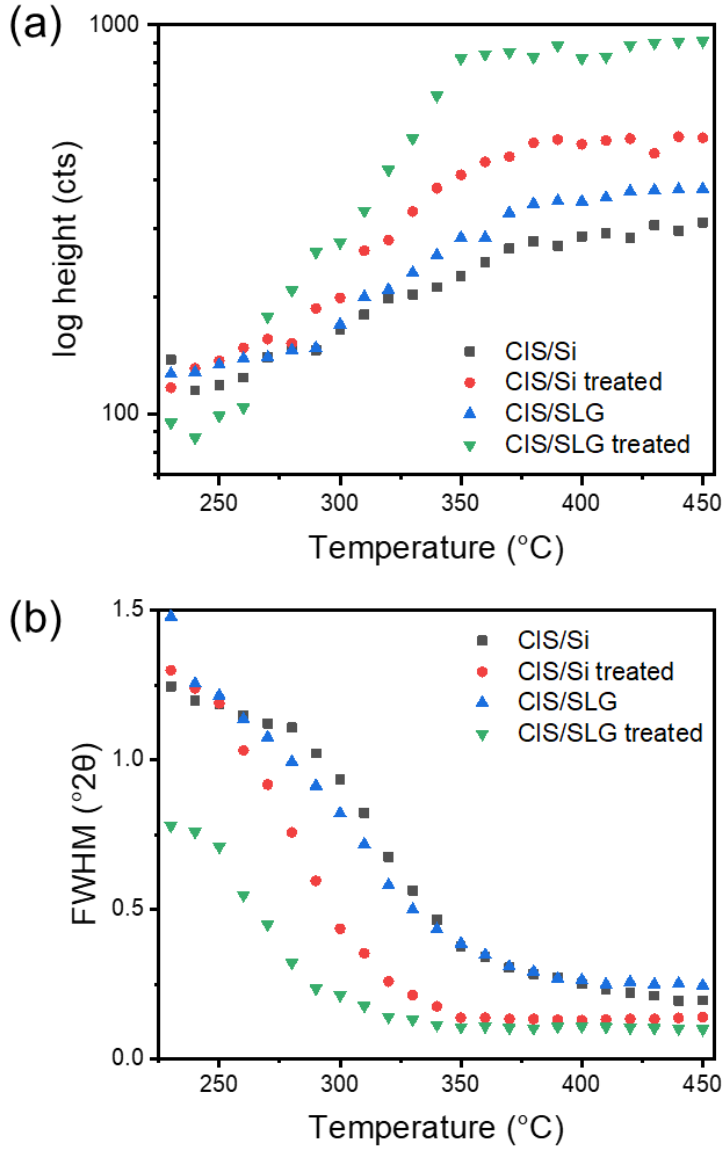

Figure 4: (a) Peak intensity, or height, in counts for the (112) orientation of $CuInSe_2$ versus temperature for all samples. (b) Five-point moving average of full-width at half maximum (FWHM) for the (112) orientation of $CuInSe_2$ versus temperature.

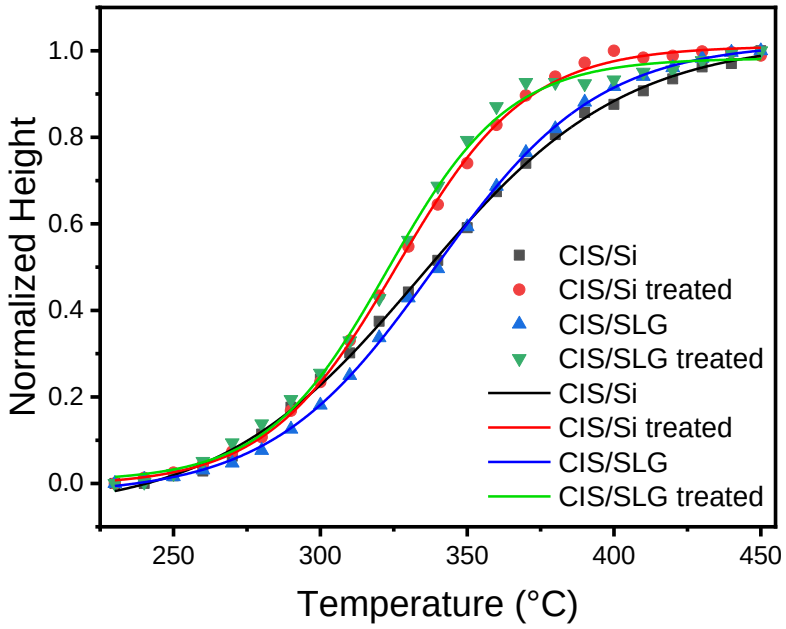

Figure 5: Five-point average of peak height data for the (112) orientation of $CuInSe_2$ normalized from zero to one (scatter points). Fitted sigmoid curves are overlain in solid lines.

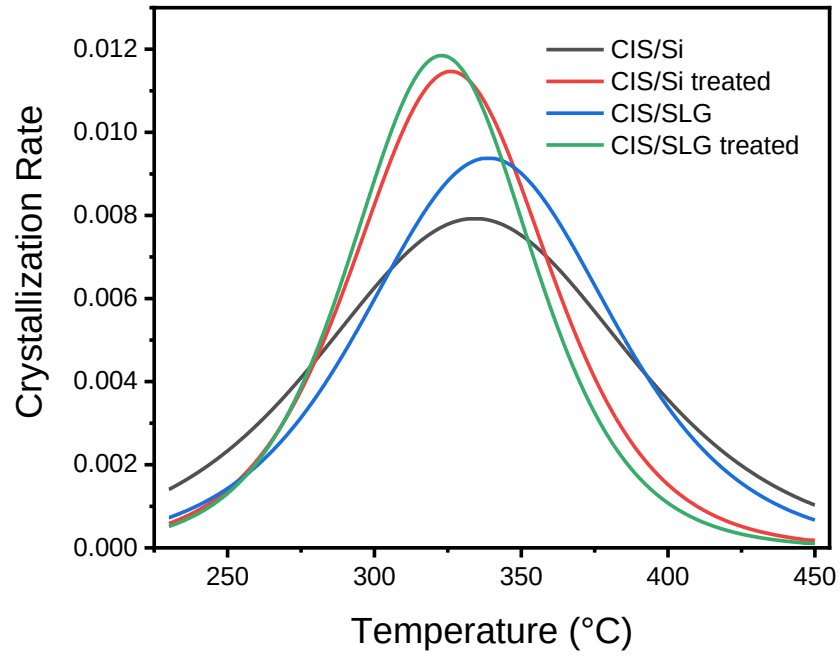

Figure 6: Crystallization rate versus temperature as determined by the first derivative of the fitted sigmoid curves of the five-point average of the normalized peak height data.

Table II – Maximum temperature values for each fitted sigmoid curves.

	T_{max} (°C)
CIS/Si	337 ± 5
CIS/Si + $InCl_3$	327 ± 5
CIS/SLG	340 ± 5
CIS/SLG + $InCl_3$	323 ± 5